Neutron drip line: Single-particle degrees of freedom and pairing properties as sources of theoretical uncertainties

A. V. Afanasjev,[1] S. E. Agbemava,[1] D. Ray,[1] and P. Ring[2]
[1]*Department of Physics and Astronomy, Mississippi State University, Mississippi State, Mississippi 39762, USA*
[2]*Fakultät für Physik, Technische Universität München, D-85748 Garching, Germany*
(Received 25 September 2014; revised manuscript received 12 December 2014; published 29 January 2015)

The sources of theoretical uncertainties in the prediction of the two-neutron drip line are analyzed in the framework of covariant density functional theory. We concentrate on single-particle and pairing properties as potential sources of these uncertainties. The major source of these uncertainties can be traced back to the differences in the underlying single-particle structure of the various covariant energy density functionals (CEDF's). It is found that the uncertainties in the description of single-particle energies at the two-neutron drip line are dominated by those existing already in known nuclei. Only approximately one-third of these uncertainties are from the uncertainties in the isovector channel of CEDF's. Thus, improving the CEDF description of single-particle energies in known nuclei will also reduce the uncertainties in the prediction of the position of the two-neutron drip line. The predictions of pairing properties in neutron-rich nuclei depend on the CEDF. Although pairing properties affect moderately the position of the two-neutron drip line they represent only a secondary source for the uncertainties in the definition of the position of the two-neutron drip line.

DOI: 10.1103/PhysRevC.91.014324 PACS number(s): 21.10.Pc, 21.60.Jz, 21.10.Dr, 21.30.Fe

I. INTRODUCTION

The analysis of theoretical uncertainties in the prediction of the position of the two-neutron and two-proton drip lines has recently attracted great interest [1–3] because of the possibility to estimate the number of nuclei which may exist in nature. Figure 1 shows an example of the nuclear landscape and related theoretical uncertainties in the definition of the position of the two-proton and two-neutron drip lines which emerge from an analysis performed in the framework of covariant density functional theory (CDFT) [4,5] using four state-of-the-art covariant energy density functionals (CEDF's). The detailed comparison of these results with the ones obtained in nonrelativistic density functional theories (DFTs) and in the microscopic+macroscopic model was already presented in Refs. [2,3]. The theoretical uncertainties for the two-neutron drip line obtained in nonrelativistic and relativistic frameworks are comparable.

One can see that the largest uncertainties exist in the position of the two-neutron drip line. Inevitably, the question about possible sources of these uncertainties emerges. Several sources have been proposed but they have not been investigated in detail. For example, the uncertainties in the position of the two-neutron drip line were related to existing uncertainties in the definition of isovector properties of the energy density functionals (EDF's) in Ref. [1]. Indeed, the isovector properties of an EDF impact the depth of the nucleonic potential with respect to the continuum, and, thus, may affect the location of two-neutron drip line. However, an inaccurate reproduction of the depth of the nucleonic potential exists in modern EDF's also in known nuclei (see the discussion in Sec. IV C of Ref. [7]). Thus, they alone cannot explain the observed features. Moreover, the observed differences in the prediction of the position of the two-neutron drip line cannot be explained by the underlying nuclear matter properties of the EDF's [3].

Note that throughout this manuscript (as in Refs. [1–3]) the position of the two-neutron drip line is specified via the two-neutron separation energy $S_{2n} = B(Z,N-2) - B(Z,N)$, the amount of energy needed to remove two neutrons. Here $B(Z,N)$ stands for the binding energy of a nucleus with Z protons and N neutrons. If the separation energy is positive, the nucleus is stable against two-neutron emission; conversely, if the separation energy is negative, the nucleus is unstable. The two-neutron drip line is reached when $S_{2n} \leqslant 0$.

Figure 1 clearly illustrates that for medium and heavy mass nuclei extreme extrapolations are necessary to reach the two-neutron drip line. This figure also suggests that only light nuclei with $Z \leqslant 28$ and medium mass nuclei with $Z \sim 38$ may be experimentally studied in the vicinity of the two-neutron drip line with future facilities such as FRIB, RIKEN, GANIL, or FAIR.

In Ref. [2] it was suggested that the position of the two-neutron drip line depends also sensitively on the underlying shell structure and the accuracy of the description of the single-particle energies. Indeed, the shell structure effects are clearly visible in the fact that for some values of the proton number Z there is basically no (or only very little) dependence of the predicted location of the two-neutron drip line on the EDF (see Fig. 1 in the present paper and Refs. [1–3]). However, no detailed study of this aspect of the problem has been performed so far.

Another interesting question is the impact of pairing and its strength on the position of the two-neutron drip line. It was found that they play an important role in the region of the drip line [8,9]. Virtual neutron pairs can be scattered to the continuum. This leads in some cases to enhanced pairing correlations and to an increasing of the binding.

The effective pairing interaction is treated in DFT in a phenomenological way with its strength fixed by a fit to experimental observables such as odd-even mass staggerings [3,10] or moments of inertia in rotating nuclei [11].

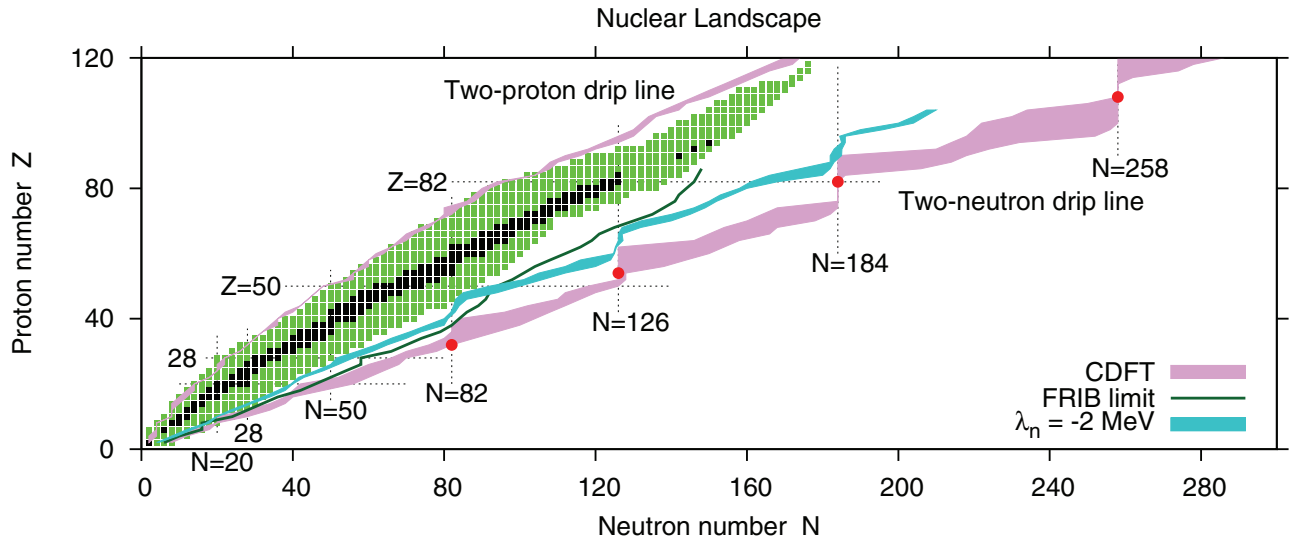

FIG. 1. (Color online) The nuclear landscape as provided by state-of-the-art CDFT calculations. The uncertainties in the location of the two-proton and two-neutron drip lines are shown by violet shaded areas. They are defined by the extremes of the predictions of the corresponding drip lines obtained with the different functionals. The uncertainties (the range of nuclei) in the location of the neutron chemical potential $\lambda_n = -2.0$ MeV are shown by the blue shaded area. Experimentally known stable and radioactive nuclei (including proton emitters) are shown by black and green squares, respectively. The green solid line shows the limits of the nuclear chart (defined as fission yield greater than 10^{-6}) which may be achieved with dedicated existence measurements at FRIB [6]. Red solid circles show the nuclei near the neutron drip line for which the single-particle properties are studied in Sec. V. The figure is partially based on the results presented in Fig. 4 of Ref. [2].

While in light nuclei the comparison with experiment in the vicinity of two-neutron drip line will be possible in future, the situation is different in medium and heavy mass nuclei for which the neutron drip line is located far away from existing or future experimental data. As a consequence, it will be impossible to verify whether the model calculations reproduce correctly the changes in pairing with increasing isospin in the experimentally unknown region of the nuclear landscape. Thus, theoretical uncertainties in the definition of pairing in such nuclei and their impact on the position of the two-neutron drip line have to be estimated.

The main goal of the current manuscript is to investigate the impact of pairing correlations and the underlying shell structure on the position of the two-neutron drip line and to outline the approaches which will allow in the future to decrease theoretical uncertainties in the definition of two-neutron drip lines.

We would like to emphasize that we discuss only *systematic* uncertainties and do not consider *statistical errors* which can be calculated from a statistical analysis during the fit [12]. Note that the number of employed covariant energy density functionals is somewhat limited and that they do not form a statistically independent ensemble because they are based on very similar terms in the CDFT Lagrangian [3]. Thus, these systematic theoretical uncertainties are only a crude approximation to the systematic theoretical errors discussed in Ref. [12].

The manuscript is organized as follows. The global behavior of pairing properties obtained in relativistic Hartree-Bogoliubov (RHB) calculations with four different CEDF's and their dependence on the specific CEDF is analyzed in Sec. II. The impact of pairing on the position of the two-neutron drip line is discussed in Sec. III. Section IV outlines the parts of the nuclear chart in which the coupling with the continuum will (or will not) affect future experimental data obtained with the next generation of experimental facilities such as FRIB. The role of the shell structure and the influence of the uncertainties in the single-particle energies on the two-neutron drip line and the uncertainties in its definition are discussed in Sec. V. Finally, Sec. VI summarizes the results of our work and gives conclusions.

II. PAIRING PROPERTIES: A GLOBAL VIEW

A. Pairing indicators

In investigations based on relativistic or nonrelativistic density functional theory it is not a trivial task to deduce from the self-consistent solutions of the Hartree-Bogoliubov or Hartree-Fock-Bogoliubov equations the size of the pairing correlations and to characterize it by one number. Apart from the trivial case of monopole pairing, where the pairing field is a multiple of unity, in calculations based on a more realistic particle-particle force the pairing field has a complicated structure. In calculation in a configuration space it is a complicated matrix with many diagonal and off-diagonal matrix elements $\Delta_{nn'}$ and in r space it is in general a nonlocal function $\Delta(\boldsymbol{r},\boldsymbol{r'})$. Only for effective interactions of zero range this reduces to a local function $\Delta(\boldsymbol{r})$.

In practice two measures for the size of pairing correlations have been used, namely, the pairing gap Δ, which represents the order parameter for the phase transition from a normal fluid to a superfluid, and the pairing energy E_{pairing}, the expectation value of the effective pairing force in the nuclear ground state. Of course, both quantities have to be given for neutrons and

protons separately and they will be discussed in detail in the present section.

In addition, pairing correlations also reveal themselves through the position of the chemical potentials for neutrons and protons and their evolution with particle number. These quantities are extremely important for the precise definition of the positions of the neutron and proton drip lines and the regions of the nuclear chart where the coupling with the continuum may become important. They will be discussed in Sec. IV.

At present, as discussed in Ref. [3], several definitions of the pairing gap Δ exist. However, the analysis presented in Sec. IV of this manuscript clearly indicates that in even-even nuclei the $\Delta_{\rm uv}$ values,

$$\Delta_{\rm uv} = \frac{\sum_k u_k v_k \Delta_k}{\sum_k u_k v_k}, \tag{1}$$

provide the best agreement with the pairing indicators deduced from odd-even mass staggerings. Here the values Δ_k are the diagonal matrix elements of the pairing field in the canonical basis [13] and the BCS occupation numbers u_k^2 and v_k^2 are calculated from the usual BCS expression,

$$\left.\begin{matrix} u_k^2 \\ v_k^2 \end{matrix}\right\} = \frac{1}{2}\left(1 \pm \frac{\epsilon_k - \lambda}{\sqrt{(\epsilon_k - \lambda)^2 + \Delta_k^2}}\right), \tag{2}$$

where $\epsilon_k = h_{kk}$ are the diagonal matrix elements of the mean field Hamiltonian in the canonical basis. The pairing gap $\Delta_{\rm uv}$ averages the matrix elements Δ_k in Eq. (1) with the weights $u_k v_k$; these are the quantities concentrated around the Fermi surface.

An alternative measure of the size of pairing correlations in theoretical calculations is the so-called pairing energy $E_{\rm pairing}$. In Hartree-(Fock)-Bogoliubov calculations it is defined as

$$E_{\rm pairing} = -\frac{1}{2}{\rm Tr}(\Delta\kappa) = -\sum_{k>0} \Delta_k u_k v_k. \tag{3}$$

Note that this is not an experimentally accessible quantity. For zero range pairing forces it has in addition the unpleasant property that it diverges with the energy cutoff, i.e., with the size of the pairing window. This can also be seen for the case of a monopole pairing force [13],

$$V^{pp} = G\, S^\dagger S, \quad \text{with} \quad S^\dagger = \sum_{k>0} a_k^\dagger a_{\bar{k}}^\dagger, \tag{4}$$

where the gap parameter,

$$\Delta = G\langle S^\dagger\rangle, \tag{5}$$

is the product of the strength G of the force and the expectation value of the pair operator $S^\dagger$,

$$\langle S^\dagger\rangle = \sum_{k>0} u_k v_k. \tag{6}$$

In this case the $\Delta_{\rm uv} = \Delta$ is finite, because for fixed size of the pairing window it is adjusted to experimental odd-even mass differences. However, $\langle S^\dagger\rangle$ diverges and G vanishes with an increasing pairing window. As a consequence the pairing energy,

$$E_{\rm pairing} = -G\langle S^\dagger\rangle\langle S\rangle = -\frac{1}{G}\Delta^2, \tag{7}$$

diverges with increasing pairing window, too. The same is true for zero range pairing forces.

From these considerations it is evident, that zero range pairing forces are reliable only in the regions where experimental gap parameters are available. Their predictive power for the regions far away from these regions might be considerably reduced (see also Ref. [14], where it was shown that the heights of fission barriers depend in the case of zero range forces on the pairing window).

B. Pairing force

To avoid the uncertainties connected with the definition of the size of the pairing window, we use in all the RHB calculations discussed in this manuscript the separable pairing interaction of finite range introduced by Tian *et al.* [15]. Its matrix elements in r space have the form,

$$V(\boldsymbol{r}_1,\boldsymbol{r}_2,\boldsymbol{r}_1',\boldsymbol{r}_2') = -f\, G\delta(\boldsymbol{R}-\boldsymbol{R'})P(r)P(r')\tfrac{1}{2}(1-P^\sigma), \tag{8}$$

with $\boldsymbol{R} = (\boldsymbol{r}_1 + \boldsymbol{r}_2)/2$ and $\boldsymbol{r} = \boldsymbol{r}_1 - \boldsymbol{r}_2$ being the center of mass and relative coordinates. The form factor $P(r)$ is of Gaussian shape,

$$P(r) = \frac{1}{(4\pi a^2)^{3/2}} e^{-r^2/4a^2}. \tag{9}$$

The two parameters $G = 738{\rm fm}^3$ and $a = 0.636$ fm of this interaction are the same for protons and neutrons and have been derived in Ref. [15] by a mapping of the ^{1}S$_0$ pairing gap of infinite nuclear matter to that of the Gogny force D1S [16].

The scaling factor f in Eq. (8) is determined by a fine tuning of the pairing strength in a comparison between experimental moments of inertia and those obtained in cranked RHB calculations with the CEDF NL3* (see Ref. [3] for details). It is fixed at $f = 1.0$ in the $Z \geqslant 88$ actinides and superheavy nuclei, at $f = 1.075$ in the $56 \leqslant Z \leqslant 76$ and at $f = 1.12$ in the $Z \leqslant 44$ nuclei. Between these regions, i.e., for $44 \leqslant Z \leqslant 56$ and for $76 \leqslant Z \leqslant 88$, the scaling factor f gradually changes with Z in a linear interpolation. The weak dependence of the scaling factor f on the CEDF was seen in the studies of pairing and rotational properties in the actinides in Refs. [11,17] and pairing gaps in spherical nuclei in Ref. [3]. Thus, the same scaling factor f as defined above for the CEDF NL3* is used in the calculations with DD-PC1, DD-ME2, and DD-MEδ. Considering the global character of this study, this is a reasonable choice.

C. Other details of the numerical calculations

In the present manuscript, the RHB framework is used for systematic studies of ground-state properties of all even-even nuclei from the proton-to-neutron drip line. We consider only axial and parity-conserving intrinsic states and solve the RHB equations in an axially deformed oscillator basis [18–20]. The truncation of the basis is performed in such a way that all states belonging to the shells up to $N_F = 20$ fermionic shells and $N_B = 20$ bosonic shells are taken into account. As tested in a

number of calculations with $N_F = 26$ and $N_B = 26$ for heavy neutron-rich nuclei, this truncation scheme provides sufficient numerical accuracy. For each nucleus the potential energy curve is obtained in a large deformation range from $\beta_2 = -0.4$ up to $\beta_2 = 1.0$ by means of a constraint on the quadrupole moment Q_{20}. Then, the correct ground-state configuration and its energy are defined; this procedure is especially important for the cases of shape coexistence.

The absolute majority of nuclei are known to be axially and reflection symmetric in their ground states [21]. The global calculations performed in the RHB framework with allowance of reflection symmetric (octupole deformed) shapes and with DD-PC1 CEDF confirm these results and clearly show that octupole deformation does not affect the ground states of the nuclei located in the vicinity of the two-neutron drip line [22]. Similar results are expected for other CEDF's. At present, triaxial RHB [23] calculations are too time-consuming to be undertaken on a global scale. However, even if triaxial deformation is present in some nuclei in the vicinity of the two-neutron drip line, its presence will not affect the conclusions obtained in the present manuscript.

D. Global pairing properties

Figure 2 compares neutron pairing energies E_{pairing} obtained with four CEDF's. In the region of known nuclei these energies are, in general, quite comparable. They are very similar in the RHB calculations with the three CEDF's DD-ME2, DD-MEδ, and DD-PC1 CEDF's with density-dependent coupling constants and slightly higher (in absolute values) in the ones with the CEDF NL3*. However, on approaching the two-neutron drip line, substantial differences develop between the pairing energies in the RHB calculations with these four CEDF's. For DD-PC1 and DD-MEδ the largest increase of neutron pairing energies is seen near the two-neutron drip line between $N = 50$ and $N = 126$; for other nuclei in the vicinity of the two-neutron drip line this increase is more modest. These increases in neutron pairing energy on approaching the two-neutron drip line become more pronounced in DD-ME2 (as compared with DD-PC1 and DD-MEδ) and they are especially pronounced in NL3*. For the latter CEDF, the absolute values of neutron pairing energies are by a factor of 3–4 higher near the two-neutron drip line than those in the known nuclei (Fig. 2). This difference reduces to a factor 2 for the DD-ME2 CEDF and becomes even smaller for the DD-MEδ and DD-PC1 CEDF's (Fig. 2). In this context we have to keep in mind that the parameter set NL3* has no density dependence in the isovector channel. Therefore, as discussed in detail in Ref. [3] the symmetry energy and the slope of the symmetry energy at saturation is considerably larger in this case than in the other three cases.

In Fig. 3 we compare for four CEDF's the evolution of the neutron pairing gaps Δ_{uv} and pairing energies E_{pairing} as a function of the neutron number in the chain of the Yb isotopes with $Z = 70$. One can see that in the RHB calculations with the three density-dependent sets DD-MEδ, DD-ME2, and DD-PC1 the pairing gaps Δ_{uv} in neutron-rich $N \geqslant 126$ nuclei have on average the same magnitude as pairing gaps in known nuclei [Fig. 3(a)]. However, the absolute pairing energies are larger by a factor of about 2 in neutron-rich nuclei as compared with the ones in known nuclei. Note that both Δ_{uv} and E_{pairing} are more or less constant in neutron-rich nuclei in the RHB calculations with DD-PC1 and DD-MEδ. On the contrary, a slight increase of the absolute values of these quantities is observed with increasing isospin in DD-ME2.

The situation is different for the CEDF NL3*. Its pairing correlations are only slightly stronger in known nuclei as compared with the density-dependent CEDF's. However, more pronounced differences are seen when the results in neutron-rich nuclei are compared with the ones in known nuclei. The pairing gaps Δ_{uv} are on average 25% larger in neutron-rich nuclei as compared with known ones and, in addition, they gradually increase with neutron number. The absolute values of the pairing energies rapidly increase with neutron number in neutron-rich $N \geqslant 126$ nuclei; near the two-proton drip line these energies are larger by a factor of 4 than average pairing energies in known nuclei.

Considering the existing differences in the Δ_{uv} and E_{pairing} values obtained in the calculations with different CEDF's in known nuclei (curves in shaded area of Fig. 3), it is important to understand to which extent the minimization of these differences will also remove the differences in these quantities in neutron-rich nuclei. To address this question, the calculations with the DD-PC1 CEDF have been performed with a pairing strength increased by 3.5%. In the region of known nuclei, the Δ_{uv} values obtained in these calculations are on average the same as the ones obtained in the calculations with NL3* CEDF [Fig. 3(a)]. The pairing energies are also similar in both calculations [Fig. 3(b)]. However, in the region of experimentally known nuclei the isospin dependencies of the quantities Δ_{uv} and E_{pairing} are slightly different in these calculations with NL3* and DD-PC1 CEDF's. These differences increase with isospin; they are especially pronounced near the two-neutron drip line. This effect may be related to different density dependence of these two CEDF's in the isovector channel.

The strong dependence of the predictions for neutron pairing on the underlying functional is also seen in the fact that Skyrme DFT calculations for the spherical nuclei with large proton gaps [9] show the reduction of neutron pairing towards the neutron drip line, which, however, is overcast by strong shell effects. This analysis is based on the Δ_{lcs} pairing gaps (for definition see Ref. [24] and Sec. IV of Ref. [3]) in even-even nuclei. However, it was found in Ref. [3] that the Δ_{uv} pairing gaps used in the present calculations reproduce the experimental odd-even mass staggerings in a considerably better way than the Δ_{lcs} pairing gaps.

E. Comments on pairing uncertainties

These results have some unpleasant consequences. First, even a careful fitting of the pairing force in known nuclei to experimental odd-even mass staggerings will not necessarily lead to a pairing force with a reliable predictive power towards the two-neutron drip line. Indeed, the Δ_{uv} and E_{pairing} values obtained in the calculations with the CEDF's NL3* and DD-PC1 (with a scaled pairing strength) differ by $\sim$30% and $\sim$100% in neutron-rich nuclei, respectively, despite the

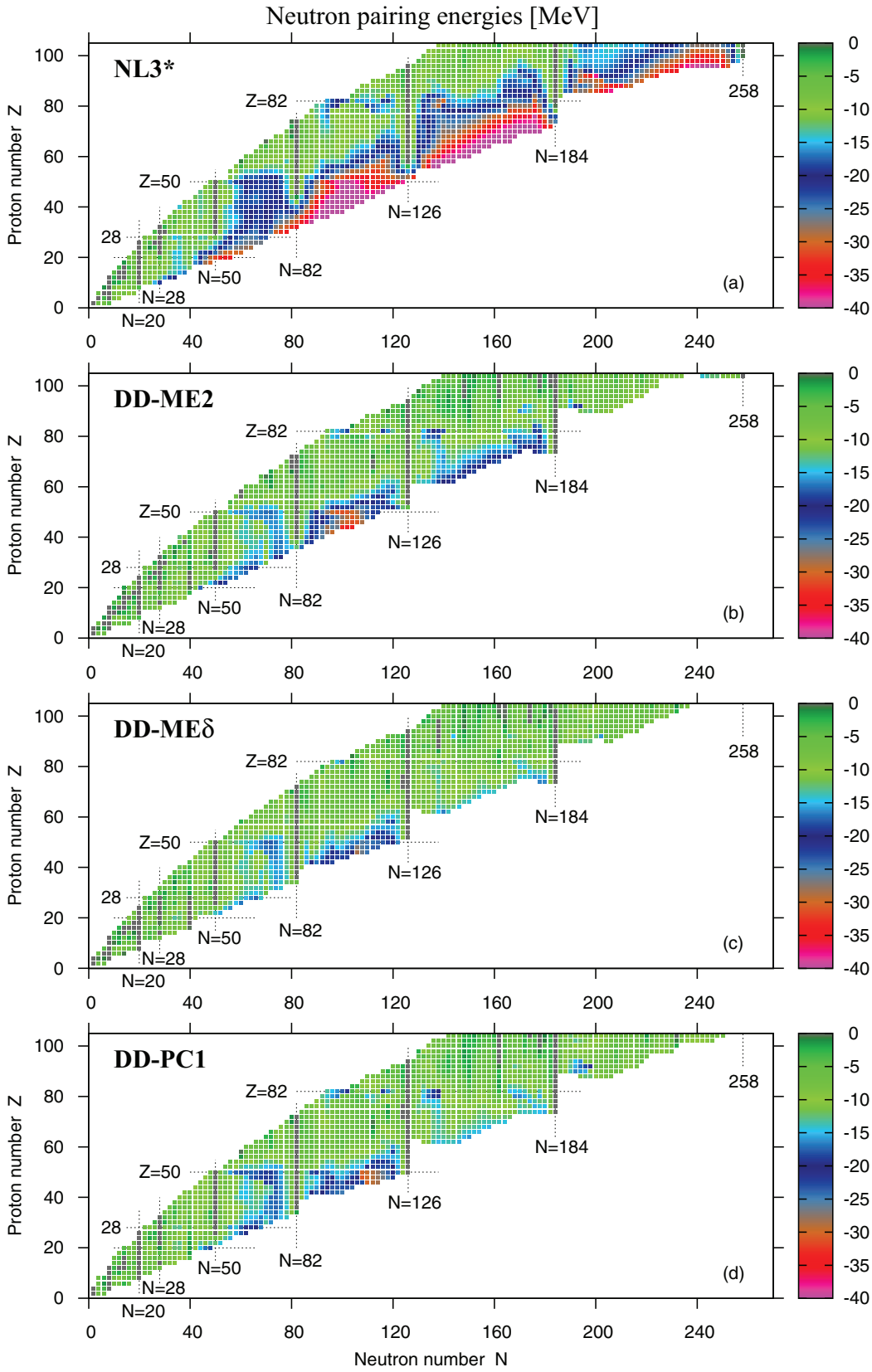

FIG. 2. (Color online) Neutron pairing energies E_{pairing} obtained in the RHB calculations with the indicated CEDF's.

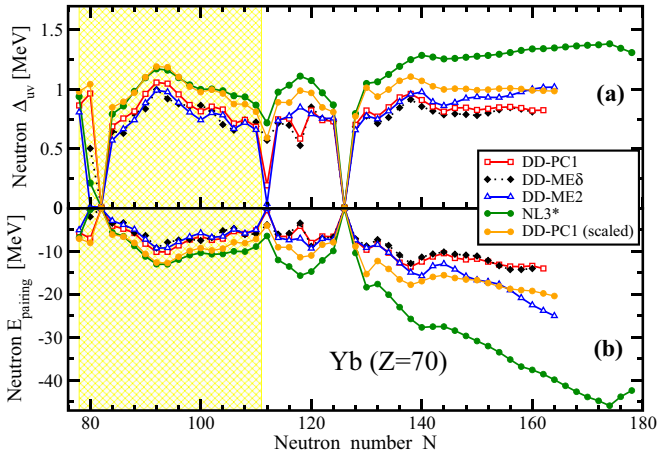

FIG. 3. (Color online) Neutron pairing gaps Δ_{uv} and pairing energies $E_{pairing}$ of the Yb nuclei located between the two-proton and two-neutron drip lines obtained in the axial RHB calculations with the indicated CEDF's. The shaded yellow area indicates experimentally known nuclei. The "DD-PC1(scaled)" curves show the results of the calculations in which the pairing strength is increased by 3.5%.

fact that they are more or less similar in known nuclei. Second, because the form of pairing force is the same in both calculations, the observed differences in the quantities Δ_{uv} and $E_{pairing}$ have to be traced back to the underlying shell structure and its evolution with neutron number. As discussed in detail in Sec. V, this is the property most poorly constrained in modern DFT's.

Note that in Ref. [3], the selection of scaling factors f for separable pairing was guided by the comparison of experimental data with different calculations based on the CEDF NL3*. The same scaling factors f were used here also in the calculations with DD-PC1, DD-ME2, and DD-MEδ. The spread in the calculated values Δ_{uv} values in known nuclei indicates that the scaling factors f used in Ref. [3] are reasonable to a within a few % (see also Sec. IV in Ref. [3] and Fig. 3 in the present paper). The weak dependence of the scaling factor f on the CEDF was already seen in the studies of pairing and rotational properties in the actinides [11,17]. Considering the global character of the study in Ref. [3], this is a reasonable choice. Definitely there are also some nuclei in which the choice of the scaling factors f is not optimal.

Figure 3 shows also some very promising facts. The predictions for pairing in nuclei with large neutron excess, i.e., far from the experimentally accessible region are very similar for the three density-dependent parameter sets DD-ME2, DD-MEδ, and DD-PC1. In particular, the results for DD-MEδ and DD-PC1 are very close. Apart from the fact that both sets are relativistic functionals these two sets are somewhat different: DD-MEδ has a finite range meson exchange and DD-PC1 has zero range, DD-MEδ was fitted to spherical nuclei, and DD-PC1 to deformed nuclei. Both of them, however, are adjusted carefully to *ab initio* calculations of nuclear matter, DD-PC1 to the nonrelativistic variational calculations of the Urbana group [25] and DD-MEδ to the nonrelativistic Brueckner-Hartree-Fock calculations of the Catania group [26] as well as to the relativistic Brueckner-Hartree-Fock calculations of the Tübingen group [27]. In addition to these *ab initio* inputs the set DD-MEδ uses only four free parameters fitted to finite nuclei. It is also seen that the parameter set DD-ME2 shows for large neutron excess slight deviations from the other two density-dependent sets. This might be connected with the fact that this CEDF has no *ab initio* input and that the proper isospin dependence is more difficult to deduce from present experimental data in nuclei located mostly in the vicinity of the valley of beta stability.

III. THE IMPACT OF PAIRING PROPERTIES ON THE POSITION OF TWO-NEUTRON DRIP LINE

A. The example of the Rn isotopes

Having in mind that there are differences in the predicted size of pairing correlations for nuclei with large neutron excess, it is important to understand how they affect the physical observables of interest, in particular the position of the two-neutron drip line. To address this question we analyze the chain of the Rn isotopes with $Z = 86$. The calculations of Refs. [2,3] show that the two-neutron drip line is located in this case at $N = 206$ for NL3* and at $N = 184$ for DD-ME2, DD-MEδ, and DD-PC1 (see Table IV in Ref. [3]).

First, we perform RHB calculations with the set NL3* and with a pairing strength decreased by 8% as compared to the one used in Ref. [3]. This brings the calculated pairing energies near the two-neutron drip line close to those obtained in the calculations with DD-ME2, DD-MEδ, and DD-PC1 [compare Figs. 2 and 4(d)]. This decrease of pairing strength has a

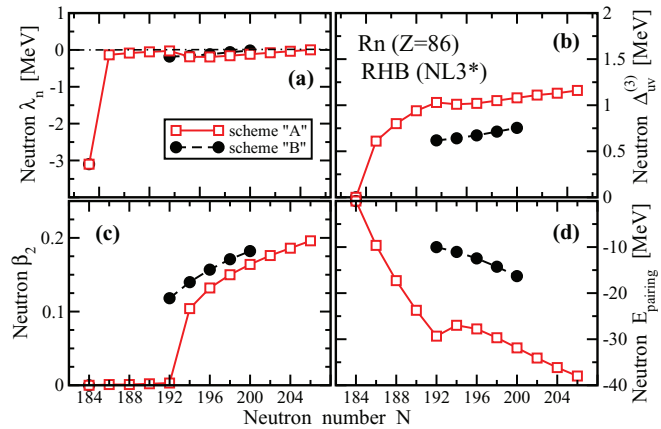

FIG. 4. (Color online) The evolution of the neutron chemical potential λ_n (a), neutron quadrupole deformation β_2 (c), neutron pairing gap Δ_{uv} (b), and neutron pairing energy $E_{pairing}$ (d) as a function of the neutron number N in the Rn isotopes with $N \geqslant 184$ obtained in RHB calculations with the CEDF NL3*. Only the results for bound nuclei are shown. The results of the calculations for two values of the strength of the pairing force [Eq. (8)] are presented. The calculational scheme labeled "A" corresponds to the pairing force with the scaling factor f defined in Sec. II B. The calculational scheme "B" uses a pairing strength reduced by 8% as compared with the scheme "A."

significant impact on the Rn isotopes near the two-neutron drip line and the position of the two-neutron drip line. Indeed, the Rn isotopes with $N = 186,188,190,202,204$, and 206, which are bound for the original pairing strength (scheme "A"), become unbound for decreased pairing (scheme "B"). Thus, the position of the two-neutron drip line located at $N = 206$ is single valued in calculational scheme A. On the contrary, in the calculational scheme B the creation of the peninsula of stability at $N = 192$–200 leads to primary (at $N = 184$) and secondary (at $N = 200$) two-neutron drip lines. In addition, the deformations of the $N = 192$–200 isotopes become larger in calculational scheme B [Fig. 4(c)]. This reflects the well-known fact that pairing typically tries to reduce the nuclear deformation.

However, the situation is more complicated. Larger pairing correlations do not necessarily shift the neutron drip line to larger neutron numbers. When we increase, for instance, in the RHB calculations with DD-ME2 and DD-PC1 the pairing strength by 8%, bringing the calculated pairing energies closer to those for NL3*, this does not affect the position of the two-neutron drip line for the chain of Rn isotopes in these CEDF's because of the details of the underlying shell structure.

The possible impact of pairing correlations on the position of the two-neutron drip line can be understood by the following arguments: The nucleus becomes unbound when the two-neutron separation energy becomes negative. In the majority of the cases (see discussion in Sec. III B) it takes place when the neutron chemical potential λ_n becomes positive. In nuclei close to the two-neutron drip line pairing correlations scatter neutron pairs from negative energy bound states into positive energy unbound states. As a consequence, the actual position of the neutron chemical potential depends on the energies of the involved levels, their degeneracy, and the strength of pairing correlations. In the extreme limit of no pairing, λ_n is equal to the negative energy of the last occupied state. For example, this takes place in the Rn isotope with $N = 184$ [Figs. 4(a) and 4(b)]. Note that the situation in nuclei with large shell gaps is very close to this limit because these gaps strongly quench pairing correlations [28]. For a realistic pairing and for a typical shell structure of nuclei close to the drip line (see, for example, Fig. 6) the neutron chemical potential will be close to the zero energy [Fig. 4(a)]. The increase of neutron number above $N = 190$ triggers the development of deformation [Fig. 4(c)] which activates a new mechanism. Now the degeneracy of states goes down from $2j + 1$ to 2 and intruder orbitals from above the gap and extruder orbitals from below the gap start to close the spherical $N = 184$ gap; this mechanism is active in the vicinity of any spherical shell gap and clearly seen in the Nilsson diagram (see, for example, Fig. 15 in Ref. [11]). This mechanism combined with the gradual increase of the deformation and neutron number allows to keep the neutron chemical potential in the vicinity of zero energy for an extended range of neutron numbers [Fig. 4(a)]. However, increasing pairing correlations produce additional binding and can shift in some cases the neutron chemical potential below zero energy thus making the nucleus bound. The opposite can happen for decreasing pairing correlations.

B. The numerical comparison of two definitions of bound and unbound nuclei and the positions of two-neutron drip line

Occasionally, in the literature the position of the two-neutron drip line is defined via the neutron chemical potential $\lambda_n = dE/dN$ as a point (nucleus) of the transition from negative λ_n ("bound" nuclei) to positive λ_n ("unbound" nuclei) values. This definition depends on the employed pairing model. In addition, it presents a linear approximation in a Taylor expansion and therefore it ignores nonlinear effects like shape changes on going from the $(Z,N-2)$ to the (Z,N) nucleus and their contribution to S_{2n}. However, this definition leads in approximately two-thirds of the cases to the same two-neutron drip line as obtained in the definition of the two-neutron drip line via the separation energies. In the remaining one-third of the cases, it leads to a two-neutron drip line which is two neutrons short of the two-neutron drip line defined via the separation energies; the nucleus which is unbound (as defined via the chemical potential) has in most of the cases a low positive value of $\lambda_n \leqslant 0.05$ MeV. Only in two cases, the difference of the positions of the two-neutron drip line, defined via the separation energies and the chemical potential, reaches four neutrons. These results were obtained from the calculations of Refs. [2,3] by analyzing the two-neutron drip line positions of 60 isotopic chains for four different CEDF's.

It is also important to mention that in the Rn isotopes discussed in the previous subsection, both definitions (via the chemical potential and via the two-neutron separation energies) give the same bound and unbound nuclei, and, thus, the same primary and secondary two-neutron drip lines. This clearly allows to trace back the distinction between bound and unbound nuclei (and thus the position of the two-neutron drip line) to the underlying single-particle structure and the properties of the pairing interaction which together define the position of chemical potential (see Sec. V D below).

C. Two-neutron drip line for the $Z = 84$–104 nuclei

To address the impact of the pairing strength on the position of the two-neutron drip line in a more global way, the two-neutron drip lines for the $Z = 82$–104 isotope chains have been studied in a similar fashion as for the Rn isotopes above. This means that the pairing strength in the RHB calculations with NL3* (DD-ME2) was decreased (increased) by 8% as compared with the one employed in Ref. [3] and the results for the two-neutron drip lines with the original and the modified strength of the pairing have been compared. These two functionals were selected because of two reasons. First, among the four CEDF's used in Refs. [2,3], the CEDF's NL3* and DD-ME2 lead to the most neutron-rich and neutron-poor two-neutron drip lines in the $Z = 82$–104 range, respectively. Second, as shown in Figs. 6(c) and 6(d), considerable similarities are seen for the neutron-single particle spectra in these two CEDF's.

Figure 5 shows the results of such a comparison. One can see that the change of the pairing strength has an impact on the two-neutron drip line. With few exceptions, stronger pairing leads to the two-neutron drip line located at larger neutron number N. However, the shift of the drip line is quite modest

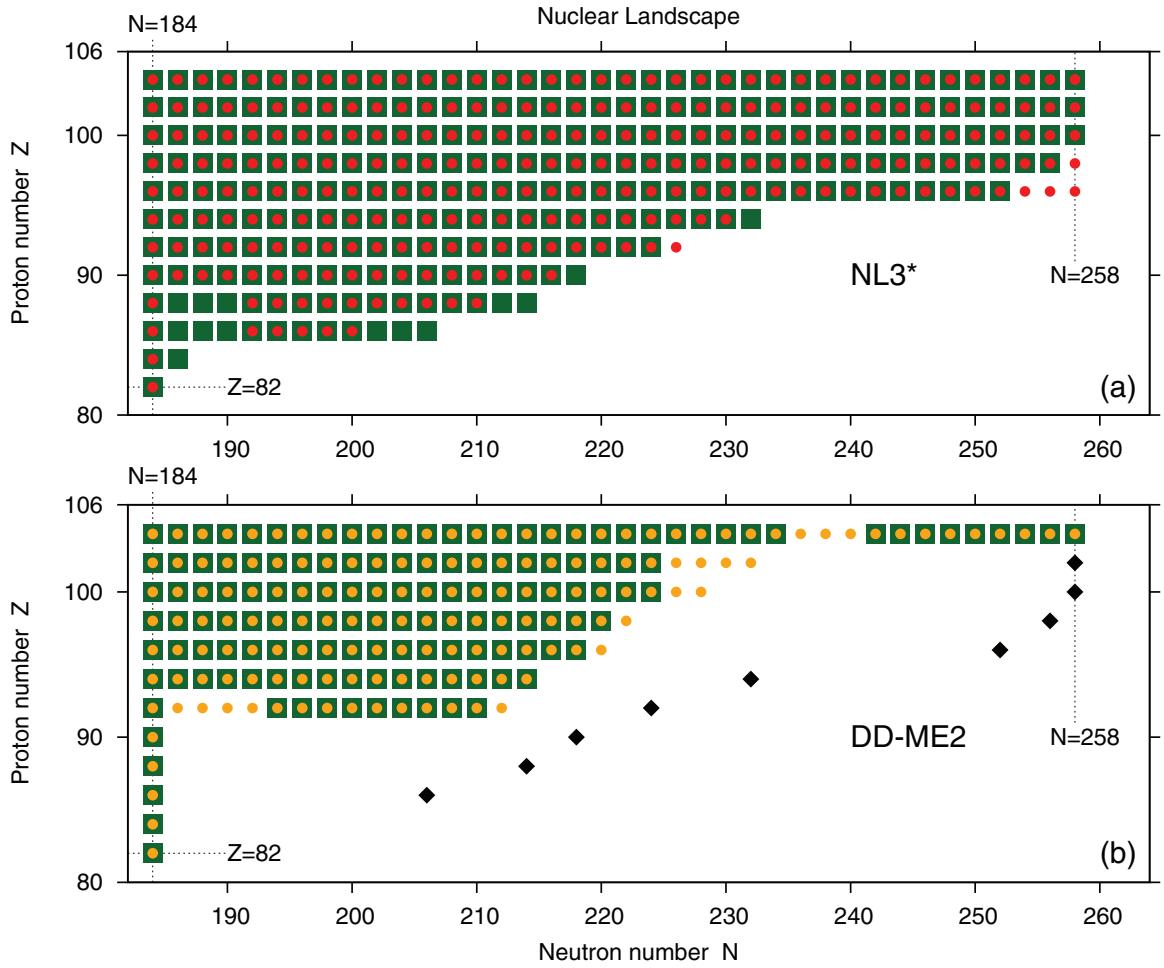

FIG. 5. (Color online) The bound nuclei in the range $82 \leqslant Z \leqslant 104$ found in RHB calculations with the CEDF's NL3* and DD-ME2. In both panels, green solid squares show the bound nuclei obtained in Ref. [3]. Red (orange) solid circles in the top (bottom) panel show the bound nuclei obtained in RHB calculations with NL3* (DD-ME2) with a pairing strength decreased (increased) by 8%. For comparison, in the bottom panel the last bound nucleus for each isotope chain obtained in Ref. [3] with the set NL3* is shown by a solid black diamond for $86 \leqslant Z \leqslant 102$; the results for $Z = 82$,84, and 104 are identical for NL3* and DD-ME2. In all calculational schemes the nuclei with $N \leqslant 184$ are bound and the ones with $N > 258$ are unbound.

for most of the values of Z. On the other hand, the peninsulas in the nuclear landscape, the physics of which was discussed in detail in Sec. IV of Ref. [3] and in Ref. [2], appear more frequently in the calculations with weaker pairing. The gaps in isotope chains, leading to such peninsulas, are present at ($Z = 92, N = 186$–192) and ($Z = 104, N = 236$–240) in the calculations with DD-ME2 [Fig. 5(b)] and at ($Z = 86, N =$ 186–190) and ($Z = 88, N = 186$–190) in the calculations with NL3* [Fig. 5(a)]. Although the pairing has an effect on the position of the two-neutron drip line, the comparison of the results obtained with the DD-ME2 and NL3* CEDF's in Fig. 5 suggests that its impact is only secondary to the one which is coming from the underlying shell structure of the functional discussed in Sec. V.

IV. LIMITS FOR THE COUPLING WITH THE CONTINUUM

Another interesting question is which future experimental data in neutron-rich nuclei will be at least moderately affected by the coupling with the continuum. If the Fermi energy is close to the continuum limit the pairing interaction causes a substantial scattering of the pairs from discrete single-particle levels below the Fermi surface to the levels in the continuum. Of course, with the present method to solve the RHB equations by an expansion in a discrete set of oscillators the details of this coupling, as, for instance, the occurrence of halo phenomena [29,30], cannot be described properly because oscillator wave functions are of Gaussian shape and decay somewhat rapidly for large radial distances. However, for the majority of nuclei with well-localized and sharply dropping density distributions at the nuclear surface, oscillator expansions have turned out to provide a very successful description of the gross properties of the coupling to the continuum. In particular, the ground states of nuclei with a Fermi level well separated from the continuum (by at least the size of the neutron pairing gap) are very well described by oscillator expansions. For medium and heavy mass nuclei the pairing gap at the Fermi surface is smaller than 2 MeV and the coupling to the continuum is strongly reduced in such cases. Thus, to have a qualitative measure for the importance of the coupling to the continuum,

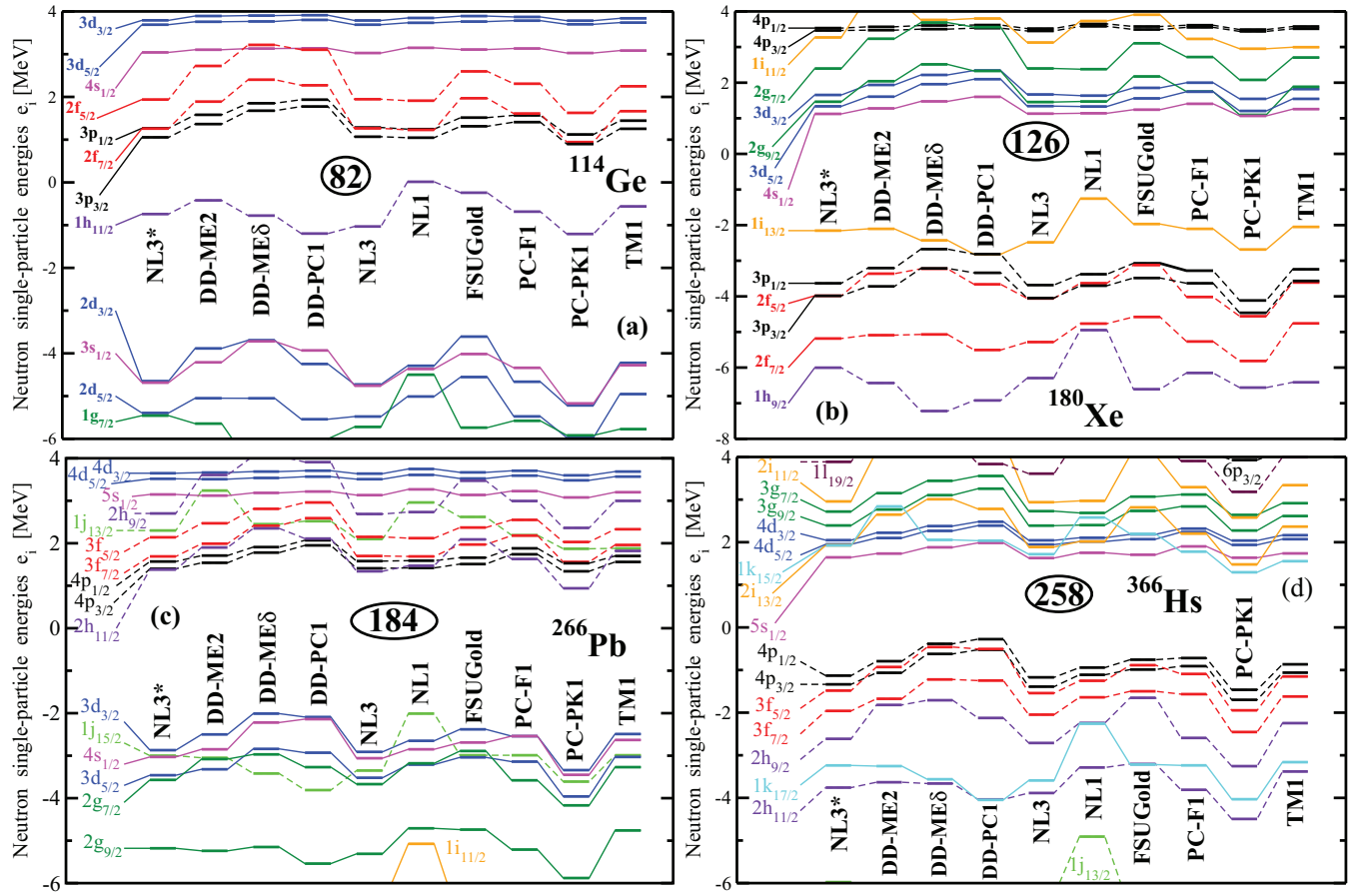

FIG. 6. (Color online) Neutron single-particle states at spherical shape in the nuclei ^{114}Ge, ^{180}Xe, ^{266}Pb, and ^{366}Hs determined with the indicated CEDF's in calculations without pairing. Solid and dashed connecting lines are used for positive and negative parity states. Spherical gaps are indicated; all the states below these gaps are occupied in the ground-state configurations.

the value of the neutron chemical potential $\lambda_n = -2.0$ MeV can be used as a safe limit for which a measurable effect of the coupling to the continuum can be expected.

We therefore compare in Fig. 1 the position of neutron chemical potential $\lambda_n = -2.0$ MeV (with its theoretical uncertainties shown by the blue shaded area) with a possible extension (green solid line) of the experimentally known part of the nuclear landscape by means of the new facilities for rare isotope beams (as, for instance, FRIB, RIKEN, GANIL or FAIR). The nuclear landscape of Fig. 1 as well as the neutron chemical potential are obtained with four state-of-the-art CEDF's (NL3*, DD-ME2, DD-PC1, and DD-MEδ) [2]. Considering the discussion above, Fig. 1 suggests that in future experiments the region of nuclei with measurable coupling with the continuum is restricted to $Z \leqslant 50$. For higher Z nuclei, future experimental data on neutron-rich nuclei can be safely treated without accounting of the coupling with the continuum.

V. SHELL STRUCTURE AND SINGLE-PARTICLE ENERGIES AT THE TWO-NEUTRON DRIP LINE.

A. Single-particle shell structure for drip line nuclei at neutron shell closures

It was suggested in Ref. [2] that the position of the two-neutron drip line sensitively depends on the underlying shell structure and that the uncertainties of the theoretical predictions of the neutron drip-line depend on the accuracy of the description of the single-particle energies. Indeed, the shell structure effects are clearly visible in the fact that for some combinations of Z and N there is basically no (or very little) dependence of the predicted location of the two-neutron drip line on the EDF [2,3] (see Fig. 1 of the present paper and Refs. [1–3]). Such a weak (or vanishing) dependence, seen in all model calculations, is especially pronounced at the spherical neutron shell closures with $N = 126$ and 184 around the proton numbers $Z = 54$ and 80, respectively. In addition, a similar situation is seen in the CDFT calculations at $N = 258$ and $Z \sim 110$ (Fig. 1).

Although it was pointed out in Ref. [2] that these features are due to the large neutron shell gaps at the magic neutron numbers, these gaps and their dependence on the CEDF have not been explored in detail. To fill this gap in our knowledge, we will perform a detailed investigation of the shell structure of nuclei in the areas where the spread in the predictions for the position of the two-neutron drip line is either nonexistent or very small. These are the nuclei $^{114}_{32}\mathrm{Ge}_{82}$, $^{180}_{54}\mathrm{Xe}_{126}$, $^{266}_{82}\mathrm{Pb}_{184}$, and $^{366}_{108}\mathrm{Hs}_{258}$ and their location in the nuclear chart is shown in Fig. 1. The neutron single-particle orbitals active in the vicinity of the Fermi level of these nuclei are shown in Fig. 6. To create a more representative statistical ensemble, the calculations have

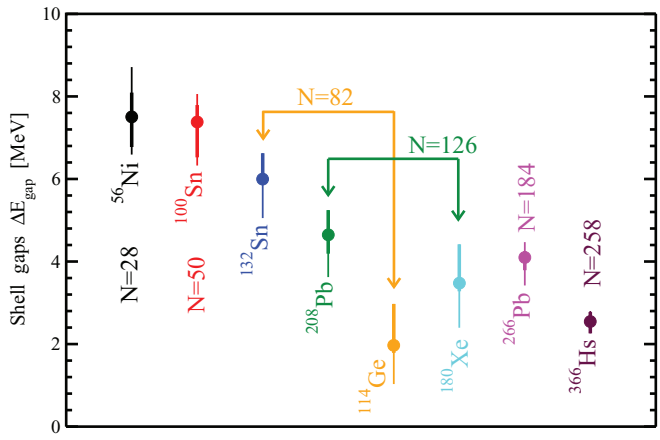

FIG. 7. (Color online) Neutron shell gaps ΔE_{gap} for the nuclei under study. The average (among 10 used CEDF's) size of the shell gap is shown by a solid circle. Thin and thick vertical lines are used to show the spread of the sizes of the calculated shell gaps; the top and bottom of these lines correspond to the largest and smallest shell gaps among the considered set of CEDF's. Thin lines show this spread for all employed CEDF's, while thick lines are used for the subset of four CEDF's (NL3*, DD-ME2, DD-MEδ, and DD-PC1). Neutron numbers corresponding to the shell gaps are indicated.

been performed with 10 CEDF's. Among those are first the CEDF's NL3* [31], DD-ME2 [32], DD-MEδ [33], and DD-PC1 [34] used earlier in Ref. [3] for a global study of the performance of the state-of-the-art CEDF's. For these CEDF's, the two-neutron drip lines are defined in model calculations up to $Z = 120$ in Refs. [2,3]. Only these four CEDF's were used in the definition of theoretical uncertainties in the position of the two-neutron drip line shown in Fig. 1. In addition, we employ now the CEDF's NL3 [35], NL1 [36], FSUGold [37], PC-F1 [38], PC-PK1 [39], and TM1 [40] in a study of the shell structure. Note that two-neutron drip lines have not been studied with these six CEDF's so far.

The results of the calculations with all these CEDF's clearly show the presence of large neutron shell gaps at $N = 126$ in ^{180}Xe, at $N = 184$ in ^{266}Pb, and at $N = 258$ in ^{366}Hs and a smaller $N = 82$ gap in ^{114}Ge (see Fig. 6). The average sizes of these gaps and the spreads in their predictions are summarized in Fig. 7. The gaps at $N = 126$ and 184 are around 4 MeV and they are the largest among these four gaps. The gap at $N = 258$ is the smallest and it is slightly larger than 2 MeV. Neutron pairing is typically quenched at these gaps (see Fig. 2). Definitely, the substantial size of the gap and the quenching of neutron pairing lead to a decrease of the uncertainties in the prediction of the two-neutron drip lines. Indeed, the largest uncertainties in the position of the two-neutron drip line exist around ^{114}Ge (Fig. 1), where the neutron $N = 82$ shell gap is the smallest among the above discussed nuclei. It is interesting that the spreads in the prediction of the size of these gaps decrease with the increase of the neutron number.

These gaps are also compared with the calculated gaps in the doubly magic nuclei ^{56}Ni, ^{100}Sn, ^{132}Sn, and ^{208}Pb (Fig. 7). The experimentally known gaps of these nuclei are reasonably well described in the relativistic calculations with particle-vibration coupling of Refs. [7,41] with the CEDF NL3*. The general trend of the decrease of the size of the neutron gaps with neutron number is clearly visible. However, the $N = 126$ gap in ^{180}Xe and the $N = 184$ gap in ^{266}Pb are only by 1 MeV smaller than the $N = 126$ gap in doubly magic ^{208}Pb. It is also important to mention that for the nuclei with $N = 82$ and $N = 126$ the spread of theoretical predictions with respect to the size of the gap only slightly increases on going from known nuclei towards nuclei in the vicinity of the two-neutron drip line. On the contrary, this spread decreases appreciably for the nuclei ^{266}Pb and ^{366}Hs as compared with lighter nuclei (Fig. 7). These results clearly suggest that the pronounced shell structure at the well-known major shells still survives in the nuclei close to the two-neutron drip line (see also an early investigation in this direction in Ref. [42]).

B. Further indicators for the two-neutron shell gap

This is also illustrated in Fig. 8 where the quantity $\delta_{2n}(Z,N)$, defined as

$$\begin{aligned}\delta_{2n}(Z,N) &= S_{2n}(Z,N) - S_{2n}(Z,N+2)\\ &= -B(Z,N-2) + 2B(Z,N) - B(Z,N+2),\end{aligned} \tag{10}$$

is shown for the four CEDF's whose global performance was studied in Ref. [3]. Here $B(N,Z)$ is the binding energy. The quantity $\delta_{2n}(Z,N)$, being related to the second derivative of the binding energy as a function of nucleon number, is a more sensitive indicator of the local decrease in the single-particle density associated with a shell gap than the two-nucleon separation energy $S_{2n}(Z,N)$.

In the literature, the quantity $\delta_{2n}(Z,N)$ is frequently called a *two-neutron shell gap*. However, as discussed in detail in Ref. [17], many factors (such as deformation changes and pairing) beyond the size of the single-particle shell gap ΔE_{gap} shown in Fig. 7 contribute to $\delta_{2n}(Z,N)$. For example, for some (Z,N) values in Fig. 8, $\delta_{2n}(Z,N)$ becomes negative because of deformation changes. Because by definition the shell gap has to be positive, it is clear that the quantity $\delta_{2n}(Z,N)$ cannot serve as an explicit measure of the size of the shell gap. However, the variations (but not their absolute values) of $\delta_{2n}(Z,N)$ and ΔE_{gap} with particle number agree rather well [17]. Thus $\delta_{2n}(Z,N)$ is still a useful quantity to see where pronounced shell gaps are located.

The quantities $\delta_{2n}(Z,N)$ for $N = 50$, which are quite large for the known nuclei (Fig. 8), decrease substantially on approaching the two-neutron drip line (at $Z = 22,24$ for DD-ME2, DD-MEδ, and DD-PC1 and at $Z = 20$–28 for NL3*). This is a reason why theoretical uncertainties in the definition of the position of the two-neutron drip line are relatively large at $N = 50$ (see Fig. 1 and Refs. [2,3]). Figures 8(b)–8(d) show that pronounced shell gaps exist at $N = 82$ and 126 in the CEDF's DD-ME2, DD-MEδ, and DD-PC1 for a large range of proton numbers Z up to the two-neutron drip line. However, on approaching the two-neutron drip line the $N = 82$ shell gap becomes smaller as compared with known nuclei for NL3* [Figs. 8(a) and Fig. 6(a)]. This again leads to a relative large theoretical uncertainty in the definition of the two-neutron drip

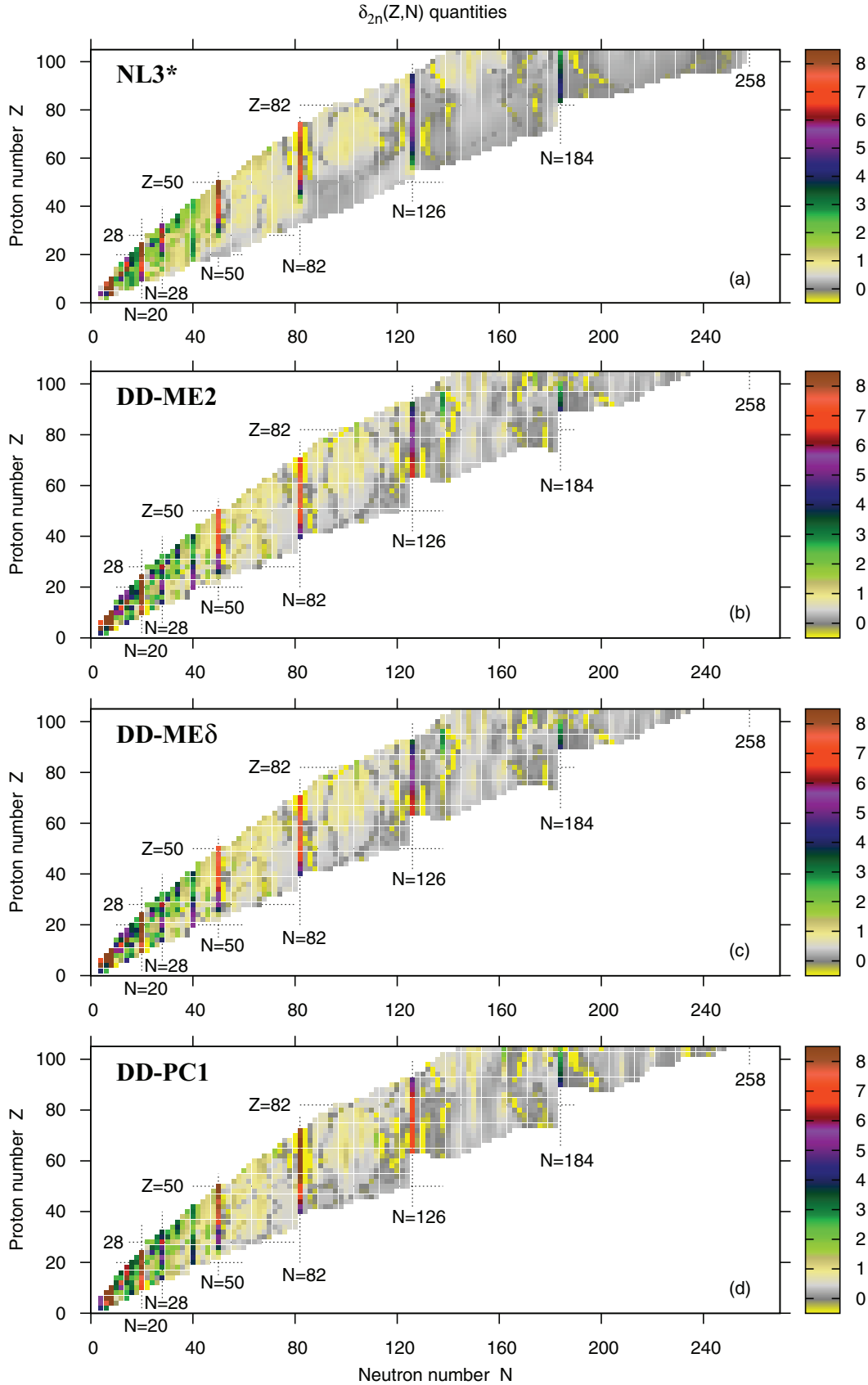

FIG. 8. (Color online) Neutron $\delta_{2n}(Z,N)$ quantities between two-proton and two-neutron drip lines obtained in RHB calculations with the indicated CEDF's.

line at $N = 82$ (see Fig. 1 and Refs. [2,3]). The corresponding uncertainty is relatively small for $N = 126$ (see Fig. 1 and Refs. [2,3]); this is because of minor differences in the size of this gap in all four CEDF's [Fig. 6(b)]. Because the shell gap for $N = 184$ is pronounced in all CEDF's near the two-neutron drip line (Fig. 8) there is no uncertainty in the definition of the two-neutron drip line at this neutron number (see Fig. 1 and Refs. [2,3]).

C. Other factors affecting the position of the two-neutron drip line

On going away from the four nuclei ^{114}Ge, ^{180}Xe, ^{266}Pb, and ^{366}Hs discussed above, other additional factors affect the position of the two-neutron drip line.

First, there is a close correlation between the nuclear deformation at the neutron-drip line and the uncertainties in the prediction of this line [2,3]. The regions of large uncertainties corresponds to transitional and deformed nuclei. This is caused by the changes in the distribution of the single-particle states induced by deformation. The spherical nuclei under discussion are characterized by large shell gaps and a clustering of highly degenerate single-particle states around them. Deformation removes this high degeneracy of the single-particle states and leads to a more equal distribution of the single-particle states with energy.

Second, the large density of the neutron single-particle states close to the neutron continuum leads to a small slope of the two-neutron separation energies S_{2n} as a function of neutron number in the vicinity of the two-neutron drip line for medium and heavy mass nuclei (see Fig. 12 in Ref. [3]). As discussed in details in Sec. VIII of Ref. [3] this translates (i) into much larger uncertainties in the definition of the position of the two-neutron drip line as compared with the two-proton drip line and (ii) into a stronger dependence of the predictions for the position of the two-neutron drip line on the accuracy of the description of the single-particle energies.

Third and most important, the position of the two-neutron drip line sensitively depends on the positions and the distribution of single-particle states around the Fermi surface, which means for nuclei close to the drip line around the continuum limit. In particular, the orbitals with high j values, known as intruder or extruder orbitals play an important role, because they usually drive deformation and, therefore, cause a considerable reordering of the single-particle spectrum. As a consequence, small differences in the single-particle spectra for the various density functionals can cause considerable effects leading to large differences in the predicted position of the two-neutron drip line.

D. A representative example of the Rn isotopes

To illustrate the factors discussed in the previous subsections we consider the chain of Rn ($Z = 86$) isotopes calculated with the CEDF NL3* and a pairing strength reduced by 8% (scheme B in the notation of Sec. III A). Moreover, we focus on the underlying single-particle structure and how its variation with particle number leads to either bound or unbound nuclei; other physical observables of this isotopic chain are discussed in Sec. III A. The evolution of the neutron single-particle states of these isotopes is shown as a function of neutron number in Fig. 9.

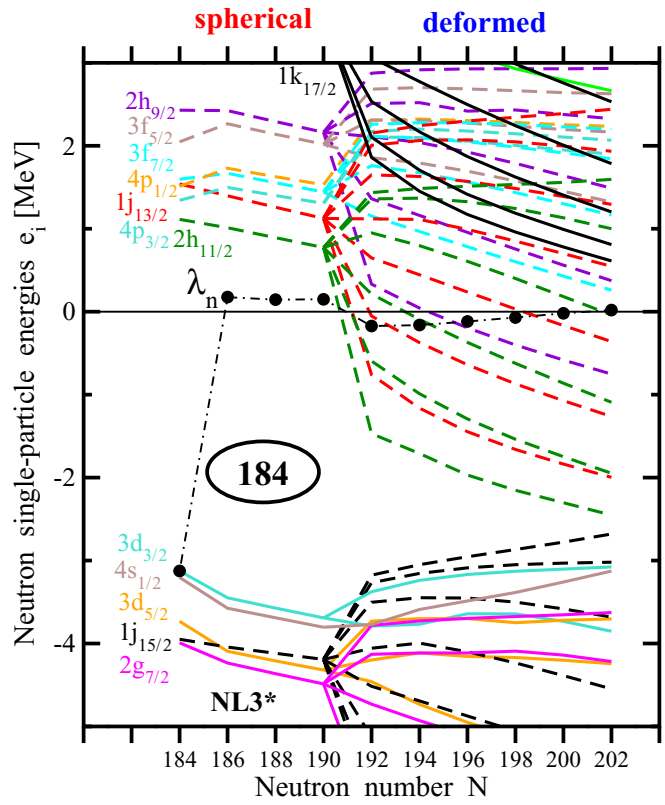

FIG. 9. (Color online) Neutron single-particle energies, i.e., diagonal elements of the single-particle Hamiltonian h in the canonical basis [13], for the ground-state configurations of the Rn isotopes calculated at their equilibrium deformations as a function of neutron number N. The neutron chemical potential λ_n is shown by a dashed-dotted line with solid circles. Note that the transition to deformation removes the $2j + 1$ degeneracy of the spherical orbitals. Solid black lines at the top of the figure are the deformed states emerging from the $1k_{17/2}$ spherical orbital. See text for further details.

The $N = 184$ isotope is spherical in the ground state and its chemical potential λ_n coincides with the energy of the last occupied single-particle orbital since neutron pairing collapses because of the large $N = 184$ shell gap. This nucleus is bound. The addition of several (two, four, and six) neutrons above this shell gap leading to the isotopes with $N = 186, 188$, and 190 restores the neutron pairing but does not affect the shape of the nucleus. However, for a given strength of pairing the chemical potential becomes positive and thus these three nuclei are unbound.

A further extension of this isotope chain to larger neutron numbers is achieved by a gradual buildup of deformation. For this process to take place the deformation driving intruder orbitals with low Ω ($\Omega = j_z$ being the projection of the single-particle angular momentum j on the symmetry axis) emerging from the high-j $2h_{11/2}, 1j_{13/2}$, and $1k_{17/2}$ spherical orbitals (located above the gap) have to be partially occupied. This indeed takes place in the RHB calculations. Note that

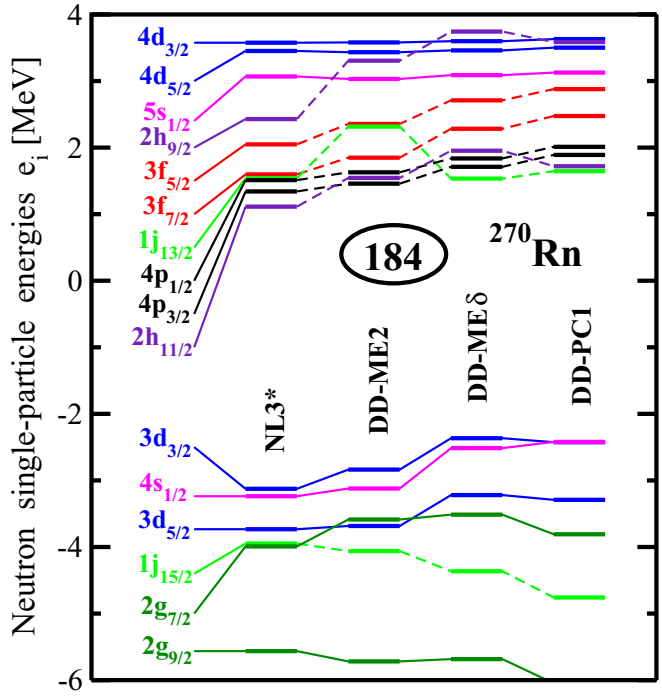

FIG. 10. (Color online) The same as Fig. 6 but for ^{270}Rn. Note that only the results for four indicated CEDF's are presented.

deformed levels with low Ω emerging from high-j orbitals come strongly down with increasing prolate deformation (see, for example, Fig. 15 in Ref. [11]). In the NL3* CEDF the energies of the spherical single-particle orbitals, from which these deformation driving intruder orbitals emerge, are such that lowering of the low Ω orbitals due to deformation triggers the chemical potential to become negative (Fig. 9). Two factors, namely, the increase of neutron number and the induced changes in single-particle structure due to deformation affect the position of chemical potential. Their delicate balance keeps the chemical potential negative up to $N = 200$ (Fig. 9). As a result, the deformed isotopes with $N = 192, 194, 196,$ and 198 are bound. However, a further increase of the neutron number leads to unbound nuclei.

The mechanism presented above is active in the nuclei with neutron numbers above $N = 184$ or $N = 258$ because several resonant high-j orbitals are located relatively low in energy with respect to the continuum limit [see Figs. 6(c) and 6(d)]. Note that, in general, the position of the Fermi level depends both on the energies of occupied single-particle states and on their occupation probabilities. As a consequence, the energies of the single-particle states below the shell gap, their occupation probabilities and their evolution with deformation are also important for the exact definition of the position of the Fermi level. In that respect it is important to mention that in some nuclei bound extruder orbitals could be as important as unbound intruder resonant orbitals for the position of the two-neutron drip line. This is because the hole states in deformed extruder orbitals with high Ω values emerging from spherical high-j orbital are as important for the creation of deformation [43] and for the definition of the position of the Fermi level as intruder orbitals with low Ω discussed above. Pair scattering from bound to resonant states creates partial holes in the extruder orbitals. The energies of these orbitals increase fast with increasing prolate deformation and this affects the position of the Fermi level. In addition, they can become unbound with increasing deformation. Such extruder orbitals are probably not that important in nuclei with N above 184 or 258 because the relevant spherical high-j orbitals $\{1j_{15/2}$ below the $N = 184$ gap [Fig. 6(c)] and $1k_{17/2}$ and $2h_{11/2}$ below the $N = 258$ gap [Fig. 6(d)]$\}$ are located too deep with respect to the relevant neutron shell gaps and the continuum limit. On the contrary, such orbitals [$1h_{11/2}$ in Fig. 6(a) and $1i_{13/2}$ in Fig. 6(b)] are important around $N = 126$ and especially around $N = 82$ because of the following reasons: (i) Their positions define the size of the gap, (ii) they are located not far away from the continuum limit, and (iii) they are reasonably well separated from bound low- and medium-j orbitals.

The current analysis also allows to understand why contrary to NL3* the chain of the Rn isotopes terminates at $N = 184$ for the CEDF's DD-ME2, DD-MEδ, and DD-PC1. The evolution of the neutron single-particle spectra as a function of neutron number in these CEDF's is similar to the one of Fig. 9. However, the neutron chemical potential never becomes negative for $N > 184$ in these three CEDF's. The reason for that is clearly seen in Fig. 10 where the spherical spectra of ^{270}Rn obtained with these CEDF's are compared with the ones obtained with NL3*. Indeed, for DD-ME2, DD-MEδ, and DD-PC1 the single-particle orbitals [especially the high-j $2h_{11/2}$ [in all three CEDF's] and the $1j_{13/2}$ (in DD-ME2) spherical orbitals from which low Ω deformation driving orbitals emerge] are located higher in energy than for NL3*. Although the shift of the single-particle energies with respect to zero energy is not very large, it is sufficient to shift the neutron chemical potential, which already fluctuates for NL3* in the energy window ±0.17 MeV for $N = 186$–202 (Fig. 9), into the positive energy range for neutron numbers above $N = 184$ for all three density dependent functionals.

E. Systematic uncertainties in the spherical shell structure

This discussion clearly shows that one needs a high predictive power for the energies of the single-particle states, in particular, for the deformation driving high-j intruder and extruder orbitals, to make reliable predictions for the location of the two-neutron drip line. In Fig. 11 we summarize the theoretical uncertainties in the description of the spherical single-particle energies shown in Fig. 6. Here all the functionals are taken into account and, therefore, these differences are substantial. In most cases they exceed 1 MeV. However, there are several states in each nucleus the energies of which depend only weakly on the CEDF (Fig. 11). These are the $4s_{1/2}$,$3d_{5/2}$, and $3d_{3/2}$ states in ^{114}Ge, $4p_{1/2}$, and $4p_{3/2}$ states in ^{180}Xe, $5s_{1/2}$,$4d_{3/2}$, and $4d_{5/2}$ states in ^{266}Pb and $5s_{1/2}$,$6p_{3/2}$, $4d_{3/2}$, and $4d_{5/2}$ states in ^{366}Hs. These are low-j positive energy states. However, in general, the spread of theoretical predictions for the energies of the single-particle

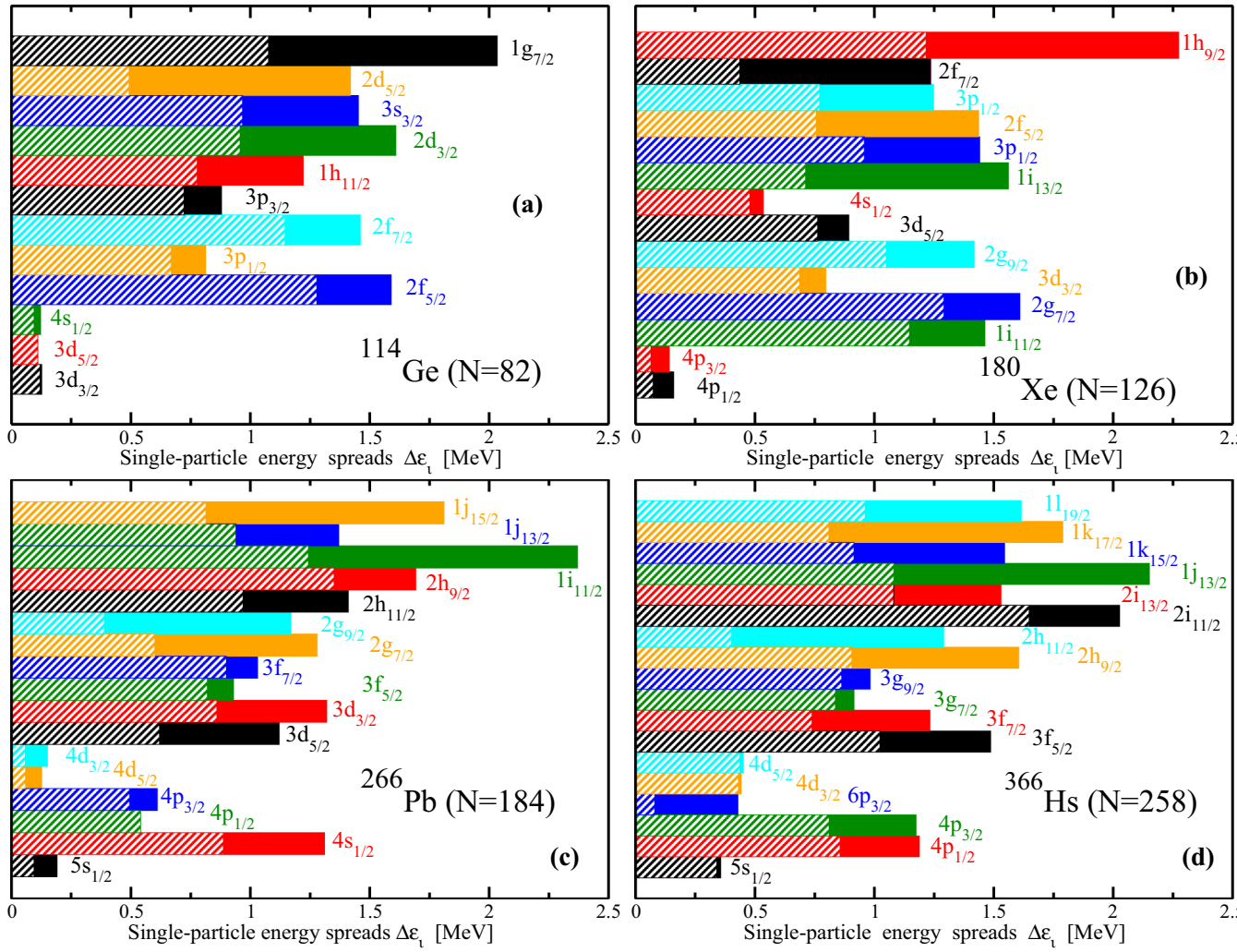

FIG. 11. (Color online) The spreads $\Delta\epsilon_i$ for the indicated neutron single-particle states in the nuclei ^{114}Ge, ^{180}Xe, ^{266}Pb, and ^{366}Hs at the two-neutron drip line. $\Delta\epsilon_i = |\epsilon_i^{\max} - \epsilon_i^{\min}|$, where $\epsilon_i^{\max}$ and $\epsilon_i^{\min}$ are the largest and smallest energies of a given single-particle state obtained with the selected set of CEDF's. The line-shaded area indicates the spreads when only the four CEDF's (namely, NL3*, DD-ME2, DD-MEδ, and DD-PC1), used in the study of Ref. [3], are considered. The combination of line-shaded and solid area shows the spreads obtained with all 10 CEDF's. The orbital angular momentum of the single-particle state increases on going from the bottom to the top of the figure. To facilitate the discussion the neutron numbers of the nuclei are shown. Based on the results presented in Fig. 6.

states increase with the increase of total angular momentum of the state.

The spread of theoretical predictions for the single-particle energies is smaller if we restrict our consideration to the last generation of CEDF's (such as NL3*, DD-ME2, DD-MEδ, and DD-PC1) for which the global performance and related theoretical uncertainties in the description of physical observables have been extensively tested in Ref. [3]. But, even for these CEDF's the uncertainties in the description of the energies of the single-particle states are in the vicinity of 1 MeV for the majority of the states.

It is interesting to compare such theoretical uncertainties in the region of the two-neutron drip line with the ones in doubly magic nuclei of a known region of the nuclear chart. Theoretical uncertainties for later nuclei (^{56}Ni, ^{100,132}Sn, and ^{208}Pb) are shown in Fig. 12. One can see that for known nuclei these theoretical uncertainties still remain substantial. However, they are by approximately 35% smaller than for the nuclei in the two-neutron drip line region. Note that only in the case of the $N = 126$ shell gap nuclei (^{180}Xe in Fig. 11 and ^{208}Pb in Fig. 12) the comparison is straightforward. This is because the same group of the single-particle states is located around the shell gap in both nuclei.

Summarizing the results of these investigations we find that for nuclei near the neutron drip line only approximately one-third of the uncertainty in the description of the single-particle energies comes from the uncertainties of the isovector properties of the EDF's. The remaining two-thirds of the uncertainties already exist in known nuclei close to the stability line. Thus, the improvement in the description of single-particle energies in known nuclei will also reduce the uncertainties in the prediction of the position of the two-neutron drip line. However, such improvement will not completely eliminate these uncertainties.

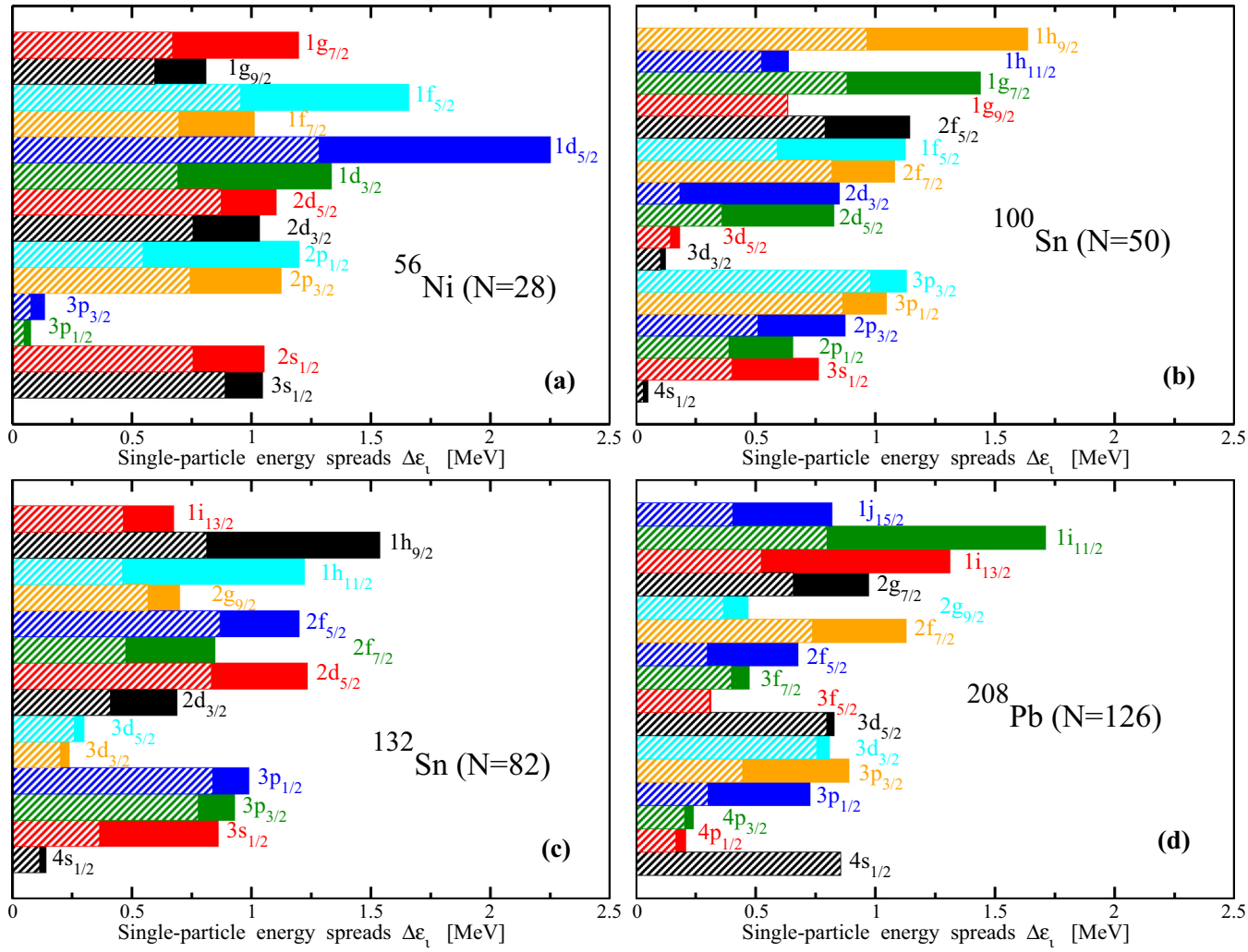

FIG. 12. (Color online) The same as in Fig. 11 but for doubly magic nuclei in an experimentally known region of the nuclear chart.

VI. CONCLUSIONS

Covariant density functional theory was applied to an analysis of sources of uncertainties in the predictions of the two-neutron drip line. The following conclusions have been obtained:

(1) The differences in the underlying single-particle structure of different covariant energy density functionals represent the major source of uncertainty in the prediction of the position of the two-neutron drip line. In particular, this position depends on the positions of high-j orbitals below the shell gap and of high-j resonances in the continuum above the shell gap. Both of them have a high degree of degeneracy at spherical shape.

(2) The analysis of the present results strongly suggests that the uncertainties in the description of the single-particle energies at the two-neutron drip line are dominated by those which already exist in known nuclei. As a consequence, only an estimated one-third of the uncertainty in the description of the single-particle energies at the two-neutron drip line could be attributed to the uncertainties in the isovector properties of EDF's. This result strongly suggests that the improvement in the DFT description of the energies of the single-particle states in known nuclei will reduce the uncertainties in the prediction of the position of the two-neutron drip line.

(3) The uncertainties in the pairing properties near the two-neutron drip line represent a secondary source of uncertainty in the definition of the two-neutron drip line. The pairing properties in neutron-rich nuclei depend substantially on the underlying CEDF, even when these properties are similar in experimentally known nuclei. For example, the pairing energies increase drastically on approaching the neutron drip line for NL3*. However, small or no increase of pairing energies is seen for DD-MEδ and for DD-PC1 in the vicinity of the neutron drip line.

These uncertainties in pairing properties translate into some uncertainties in the position of the two-neutron drip line. However, they are substantially smaller than the ones from the underlying single-particle structure.

During the last several years considerable progress was achieved in our understanding of the global performance of state-of-the-art covariant energy density functionals and the corresponding theoretical uncertainties. Many physical observables related to the ground-state properties (binding energies, charge radii, deformations, neutron skin thicknesses, the positions of drip lines, etc., [3]) and the properties of excited states (moments of inertia [11], the energies of (predominantly) single-particle states [7,41,44], fission barriers [45,46], etc.) have been studied either globally or at least systematically in a specific region of the nuclear chart. Theoretical uncertainties for many physical observables have been defined.

A careful and systematic comparison of these results with available experimental data clearly shows that in many cases the discrepancies between theory and experiment are caused by a nonoptimal description of the single-particle energies [47]. This is not surprising considering that the current generation of CEDF's was fitted only to bulk and nuclear matter properties. As a consequence, density functional theory provides a less accurate description of the single-particle energies as compared to microscopic+macroscopic models [43,48,49] with phenomenological potentials such as Folded Yukawa, Woods-Saxon or Nilsson (see Ref. [44] and references quoted therein) the parameters of which are directly adjusted to experimental data on single-particle energies. The existing discrepancies between theory and experiment clearly indicate the need for an improvement of the description of the single-particle energies in CDFT.

This probably cannot be achieved just by fitting theoretical single-particle energies to experimental data because many of the experimental single-particle states are strongly fragmented by particle-vibrational coupling, in particular in spherical nuclei [7,41]. Therefore, the inclusion of the single-particle information into the fitting protocols of CEDF's is at the moment at its infancy [47,50]. A reasonable procedure needs first a satisfying description of low-lying collective states in nuclei and their coupling to the single-particle states. This is definitely difficult, in particular in deformed nuclei, but it also includes a problem of self-consistency because the low-lying vibrations depend on the single-particle structure in the neighborhood of the Fermi level [51]. In any case, such an approach requires a systematic and comparative study of the influence of tensor forces [50] and particle-vibrational coupling [51]. Therefore, as illustrated, for example, in Skyrme DFT [52,53] there is a limit of accuracy for the description of single-particle energies which can be achieved at the DFT level. So far, similar investigations are missing in deformed nuclei.

Although the present investigation is restricted to covariant energy density functionals, it is reasonable to expect that its results are in many respects also applicable to nonrelativistic DFTs. This is because similar problems in the description of single-particle and pairing properties exist also for the Skyrme and Gogny DFTs [10,52–54].

ACKNOWLEDGMENTS

This material is based upon work supported by the U.S. Department of Energy, Office of Science, Office of Nuclear Physics under Awards No. DE-FG02-07ER41459 and No. DE-SC0013037 and by the DFG cluster of excellence "Origin and Structure of the Universe" (www.universe-cluster.de).

[1] J. Erler, N. Birge, M. Kortelainen, W. Nazarewicz, E. Olsen, A. M. Perhac, and M. Stoitsov, Nature (London) **486**, 509 (2012).
[2] A. V. Afanasjev, S. E. Agbemava, D. Ray, and P. Ring, Phys. Lett. B **726**, 680 (2013).
[3] S. E. Agbemava, A. V. Afanasjev, D. Ray, and P. Ring, Phys. Rev. C **89**, 054320 (2014).
[4] P. Ring, Prog. Part. Nucl. Phys. **37** 193 (1996).
[5] D. Vretenar, A. V. Afanasjev, G. A. Lalazissis, and P. Ring, Phys. Rep. **409**, 101 (2005).
[6] H. Schatz (private communication, 2014); see also [https://groups.nscl.msu.edu/frib/rates/fribrates.html].
[7] E. V. Litvinova and A. V. Afanasjev, Phys. Rev. C **84**, 014305 (2011).
[8] G. F. Bertsch and H. Esbensen, Ann. Phys. (NY) **209**, 327 (1991).
[9] A. Pastore, J. Margueron, P. Schuck, and X. Viñas, Phys. Rev. C **88**, 034314 (2013).
[10] M. Bender, K. Rutz, P.-G. Reinhard, and J. A. Maruhn, Eur. Phys. J. A **8**, 59 (2000).
[11] A. V. Afanasjev and O. Abdurazakov, Phys. Rev. C **88**, 014320 (2013).
[12] J. Dobaczewski, W. Nazarewicz, and P.-G. Reinhard, J. Phys. G **41**, 074001 (2014).
[13] P. Ring and P. Schuck, *The Nuclear Many-Body Problem* (Springer-Verlag, Berlin) (1980).
[14] S. Karatzikos, A. V. Afanasjev, and P. R. G. A. Lalazissis, Phys. Lett. B **689**, 72 (2010).
[15] Y. Tian, Z. Y. Ma, and P. Ring, Phys. Lett. B **676**, 44 (2009).
[16] J. F. Berger, M. Girod, and D. Gogny, Comput. Phys. Commun. **63**, 365 (1991).
[17] A. V. Afanasjev, T. L. Khoo, S. Frauendorf, G. A. Lalazissis, and I. Ahmad, Phys. Rev. C **67**, 024309 (2003).
[18] Y. K. Gambhir, P. Ring, and A. Thimet, Ann. Phys. (NY) **198**, 132 (1990).
[19] P. Ring, Y. K. Gambhir, and G. A. Lalazissis, Comput. Phys. Commun. **105**, 77 (1997).
[20] T. Niksic, N. Paar, D. Vretenar, and P. Ring, Comput. Phys. Commun. **185**, 1808 (2014).
[21] P. Moeller, R. Bengtsson, B. Carlsson, P. Olivius, T. Ichikawa, H. Sagawa, and A. Iwamoto, At. Data Nucl. Data Tables **94**, 758 (2008). .
[22] S. Agbemava, A. V. Afanasjev, and P. Ring (unpublished).
[23] A. V. Afanasjev, P. Ring, and J. König, Nucl. Phys. A **676**, 196 (2000).
[24] T. Duguet, P. Bonche, P.-H. Heenen, and J. Meyer, Phys. Rev. C **65**, 014310 (2001).

[25] A. Akmal, V. R. Pandharipande, and D. G. Ravenhall, Phys. Rev. C **58**, 1804 (1998).
[26] M. Baldo, C. Maieron, P. Schuck, and X. Viñas, Nucl. Phys. A **736**, 241 (2004).
[27] E. N. E. van Dalen, C. Fuchs, and A. Faessler, Eur. Phys. J. A **31**, 29 (2007).
[28] Y. R. Shimizu, J. D. Garrett, R. A. Broglia, M. Gallardo, and E. Vigezzi, Rev. Mod. Phys. **61**, 131 (1989).
[29] J. Meng and P. Ring, Phys. Rev. Lett. **77**, 3963 (1996).
[30] L. Li, J. Meng, P. Ring, E.-G. Zhao, and S.-G. Zhou, Phys. Rev. C **85**, 024312 (2012).
[31] G. A. Lalazissis, S. Karatzikos, R. Fossion, D. P. Arteaga, A. V. Afanasjev, and P. Ring, Phys. Lett. B **671**, 36 (2009).
[32] G. A. Lalazissis, T. Nikšić, D. Vretenar, and P. Ring, Phys. Rev. C **71**, 024312 (2005).
[33] X. Roca-Maza, X. Viñas, M. Centelles, P. Ring, and P. Schuck, Phys. Rev. C **84**, 054309 (2011).
[34] T. Nikšić, D. Vretenar, and P. Ring, Phys. Rev. C **78**, 034318 (2008).
[35] G. A. Lalazissis, J. König, and P. Ring, Phys. Rev. C **55**, 540 (1997).
[36] P.-G. Reinhard, M. Rufa, J. Maruhn, W. Greiner, and J. Friedrich, Z. Phys. A **323**, 13 (1986).
[37] B. G. Todd-Rutel and J. Piekarewicz, Phys. Rev. Lett. **95**, 122501 (2005).
[38] T. Bürvenich, D. G. Madland, J. A. Maruhn, and P.-G. Reinhard, Phys. Rev. C **65**, 044308 (2002).
[39] P. W. Zhao, Z. P. Li, J. M. Yao, and J. Meng, Phys. Rev. C **82**, 054319 (2010).
[40] Y. Sugahara and H. Toki, Nucl. Phys. A **579**, 557 (1994).
[41] E. Litvinova and P. Ring, Phys. Rev. C **73**, 044328 (2006).
[42] M. M. Sharma, G. A. Lalazissis, W. Hillebrandt, and P. Ring, Phys. Rev. Lett. **72**, 1431 (1994).
[43] A. V. Afanasjev, D. B. Fossan, G. J. Lane, and I. Ragnarsson, Phys. Rep. **322**, 1 (1999).
[44] A. V. Afanasjev and S. Shawaqfeh, Phys. Lett. B **706**, 177 (2011).
[45] H. Abusara, A. V. Afanasjev, and P. Ring, Phys. Rev. C **82**, 044303 (2010).
[46] B.-N. Lu, E.-G. Zhao, and S.-G. Zhou, Phys. Rev. C **85**, 011301 (2012).
[47] A. V. Afanasjev, arXiv:1409.4853 [J. Phys. G (to be published)].
[48] P. Möller, J. R. Nix, W. D. Myers, and W. J. Swiatecki, At. Data Nucl. Data Table **59**, 185 (1995).
[49] K. Pomorski and J. Dudek, Phys. Rev. C **67**, 044316 (2003).
[50] G. A. Lalazissis, S. Karatzikos, M. Serra, T. Otsuka, and P. Ring, Phys. Rev. C **80**, 041301 (2009).
[51] A. V. Afanasjev and E. Litvinova, arXiv:1409.4855.
[52] M. Kortelainen, J. Dobaczewski, K. Mizuyama, and J. Toivanen, Phys. Rev. C **77**, 064307 (2008).
[53] M. Kortelainen, J. McDonnell, W. Nazarewicz, E. Olsen, P.-G. Reinhard, J. Sarich, N. Schunck, S. M. Wild, D. Davesne, J. Erler, and A. Pastore, Phys. Rev. C **89**, 054314 (2014).
[54] M. Bender, P.-H. Heenen, and P.-G. Reinhard, Rev. Mod. Phys. **75**, 121 (2003).